SIGNAL PROCESSING

Signal Processing 82 (2002) 527–544

An edge preserving noise smoothing technique using multiscale morphology

S. Mukhopadhyay, B. Chanda *

Electronics and Communication Sciences Unit, Indian Statistical Institute, Calcutta 700035, India

Received 4 January 2000; received in revised form 10 August 2000; accepted 9 July 2001

Abstract

This paper presents a method for improving the quality of gray-level images by reducing the effect of noise using multiscale morphology. The underlying concept of the work is to assign progressively less importance to features of smaller scales as their possibilities of being noise particles are more. Features at various scales are extracted by means of morphological filtering. The proposed scheme is first illustrated in one dimension. Morphological towers are built to implement the method in two dimensions. The proposed algorithm has been tested on a set of real images corrupted with different types of noise. The results are compared with those of other standard noise removal algorithms based on some standard performance measures. A modification of the method considering noise statistics along with its results are also presented in this paper.

Keywords: Mathematical morphology; Multiscale morphology; Morphological towers; Noise smoothing

1. Introduction

A very common source of degradation in a digital image is noise contamination. Noise may be present in an image due to different reasons and its effect in degrading the image is different for different kind of noise. The image corrupted with noise generally suffers from having low *signal-to-noise* ratio and may not be suitable for further processing without removing or reducing the effect of noise in it. For example, a biomedical image corrupted with noise cannot be used reliably for clinical diagnosis of disease. A satellite image corrupted with speckle noise fails to represent the remote-sensed data of, say, a geographical terrain. Hence removal of noise from the image is of utmost importance in image processing and analysis. However, removal of noise by every known noise cleaning algorithm is associated with partial removal of the desired signal component also. For example, *mean filters* generally blur the edges and the corner points present in the image.

Since the removal of noise may affect information content of the image it becomes quite relevant to deal with the behavior of the noise. This mainly includes statistical modeling, analysis and estimation of the associated noise. Most often the exact nature or type of the noise are not known beforehand. However, the type of noise degrading the image is dependent on the imaging system. Accordingly a suitable mathematical or statistical noise model may be fit to quantify or estimate the parameters of the model. The statistical behavior of noise is generally described by a probability density function. The noise process may be linear or non-linear and the noise may be additive or

multiplicative. The noise may be signal dependent or signal independent as well. As a result, a noise removal scheme or algorithm cannot be identically efficient in removing all kinds of noise from images.

There are various noise removal schemes each having their own merits and demerits. Some of these are spatial domain techniques while others are frequency domain techniques. The spatial domain techniques, usually, smooth noise by employing the knowledge acquired from the neighborhood of each pixel in the noisy image. For example, the well known *mean filter* [29] replaces intensity at each pixel of the noise corrupted image by the average intensity computed over a prescribed neighborhood. In other variants of mean filters this average is computed by assigning intuitive weightages to the pixels contained in the neighborhood. *Median filters* [29], on the other hand, compute median in lieu of the average. While mean filters have the problem of blurring the edges present in the image, median filters, by and large, preserve them by reducing the effect of statistical outliers present in the local neighborhood. Crimmins [8] developed a geometric filter which has proved to be efficient in removing speckle noise from satellite image data. Restoring an image from its noisy version is performed in frequency domain by means of *low pass filtering*, *inverse filtering*, *Wiener filtering* [29]. However, almost all conventional noise removal algorithms mentioned above do not take care of shapes and scales of the objects or features present in the image.

The application of *mathematical morphology* [23,35] to image processing and analysis has initiated a new approach for solving a number of problems. This approach is based on set theoretic concepts of shape. The speciality of morphological processing is that it treats the objects present in an image as sets. The identification of objects and object features through their shapes makes mathematical morphology a useful approach for various machine vision systems and recognition processes. The popularity of morphological processing has led to hardware implementation of morphological operators. These include Golay logic processor [12], Leitz texture analysis system (TAS) [17], CLIP processor arrays [9], and Delft image processor DIP [19]. The extension of concepts of morphological operations like dilation and erosion (also known as Minkowski addition and subtraction [25], respectively) of binary objects to the arena of gray level images using max and min operations may be found in [37,15]. Since its inception mathematical morphology has observed a steady growth, and during last two decades various morphological operators and processing techniques have been proposed. These include area (size) morphology [40,41], soft morphology [11,28], regulated morphology [10], directional morphology [1], etc. Morphological operations are interpreted as set–set processing, function–function processing, function–set processing [21], etc.

Morphological techniques are being used for solving various image processing problems including noise smoothing. The most common noise removal techniques using mathematical morphology are *opening* and *closing* [14] or their cascades known as *alternating sequential filters* [36]. Safa and Flouziat [30] have used mathematical morphology in removing speckle from radar images. Schonfeld and Goutsias [33] have done an optimal morphological pattern restoration from noisy binary images. Lin et al. [7] have used morphology in reducing noise of VQ encoded images through anti-gray coding. A scheme for morphological anisotropic diffusion for smoothing noise from gray-scale images has been suggested by Segall and Acton [34]. In this paper we have devised a noise smoothing technique using multiscale morphology that also preserve edges. In the following description we use similar notations of digital image processing and mathematical morphology as used in [14]. Section 2 gives a brief discussion on mathematical morphology and multiscale morphology. In Section 3 we have described the proposed method. Section 3.1 describes the theoretical formulation of noise smoothing technique using multiscale morphology. Section 3.2 gives a simplified illustration of the proposed formulation on one-dimensional function. Section 3.3 presents elaborately various steps of the implementation of the proposed algorithm. The experimental results and discussions are given in Section 4. A modification of the proposed scheme considering the noise statistics is presented in Section 5. Finally, concluding remarks are given in Section 6.

2. Multiscale morphology

Mathematical morphology is a potential tool for solving a wide range of problems in the field of image

processing and computer vision. It is used for extracting, modifying and combining image features that are useful in the representation and description of objects or shapes. Morphological operations are by and large set theoretic operations defined between two sets: the object and the structuring element (SE) [35,14]. The shape and the size of SE play crucial roles in such types of processing and are therefore chosen according to the associated application. The two basic morphological operations are *erosion* and *dilation*, and the opening (closing) operation is the sequential combination of erosion (dilation) and dilation (erosion). In this work, we adopt, the *function- and set-processing* (FSP) system an elaborate description of which may be found in [21]. FSP dilation of a gray-level image $g(r,c)$ by a two-dimensional point set B is defined as

$$(g \oplus B)(r,c) = \max_{(k,l)\in B} \{g(r-k, c-l)\}. \tag{1}$$

Similarly, FSP erosion of $g(x, y)$ by B is defined as

$$(g \ominus B)(r,c) = \min_{(k,l)\in B} \{g(r+k, c+l)\}. \tag{2}$$

The shape of the structuring element B plays an important role in extracting or processing shape-based features or objects present in the image. An SE of a given shape, however, cannot treat objects of similar shape, but of varying size identically. Thus, for a categorical processing based on the shape as well as size of objects in the image, we incorporate a second attribute to the structuring element called *scale*. A family of SEs consisting of the primitive SE and its higher order homothetics is capable of processing features based on shape and size. Such a scheme of morphological operations where a structuring element of varying scale is utilized is termed as *multiscale morphology* [35,21]. Multiscale opening and closing [38] are defined, respectively, as

$$(g \circ nB)(r,c) = ((g \ominus nB) \oplus nB)(r,c), \tag{3}$$

$$(g \bullet nB)(r,c) = ((g \oplus nB) \ominus nB)(r,c), \tag{4}$$

where B is a point set representing the structuring element of a definite shape and n is an integer representing the scale factor of the structuring element. If B is convex, we obtain nB by dilating B recursively $n-1$ times with itself as shown below.

$$nB = \underbrace{B \oplus B \oplus B \oplus \cdots \oplus B}_{n-1 \text{ times}}. \tag{5}$$

By convention $nB = \{(0,0)\}$ when $n = 0$. Multiscale processing system should have the properties like (i) *causality* and (ii) *edge localization* [27,20,3]. By the term 'causality' we mean no regional extrema and, consequently, no edge is introduced as the scale increases. 'Edge localization' means an edge should not drift from its original position. The system is also expected to be *scale-calibrated*, i.e. at a particular scale, all features of only that scale are present in the output image.

The multiscale opening produces flat regions by removing bright objects or its parts smaller than the SE. The properties: $g \circ B \leqslant g$ and $g \circ iB \geqslant g \circ jB$ for $i < j$ imply that new relatively darker pixels may result at higher scales due to opening. In the case of multiscale closing, new relatively brighter pixels may result at higher scales. Secondly, removal of parts of an object introduces new edges. Thus, conventional opening and closing do not satisfy the causality property. This is elaborated in the next paragraph.

The basic assumption that the proposed algorithm takes in smoothing noise is that the image contains planar intensity patches corrupted with noise grains. In one dimension, a translation invariant morphological operator preserves the slope of the signal [4]. In fact, a 'single-slope signal' — linear function — is left unchanged by any morphological operator with the exception of a translation of the function. However, in case of opening with a horizontal straight line segment, i.e. the SE, the edges are first drifted inward due to erosion which is followed by dilation that drifts the edges outward by the same amount. This avoids any displacement of edges. In the case of non-linear functions some peaks having width smaller than the length of the SE vanish completely. As a result, some edges may not be present in the opened image. However, other edges are present in their original positions. In the case of two or higher dimensions the situation is not, in general, so. Since we are dealing with image processing problems, our discussion is confined to two dimensions only. The SE we use is a disk of certain radius. Aforementioned analysis is valid (i.e., edge localization problem does not arise) only where the radius of curvature of the

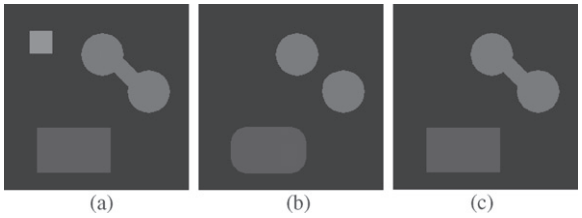

Fig. 1. (a) Original image; (b) result of conventional opening of (a) using a disk SE; and (c) result of opening by reconstruction of (a) with same SE.

edges is not less than that of the SE or the features are not too narrow [6]. Otherwise, the features are either completely removed or pruned. In the latter case we see the edges are drifted inwards. For example, if a rectangle is opened with a disk SE of diameter less than the smaller side of the rectangle, the rectangle is pruned at its corners. As a result, corner edges are drifted inwards introducing an edge localization problem [see Fig. 1(a) and (b)]. Similar analysis holds for closing also in the complement sense. Bangham et al. [3] suggested a scale-space operator, called M- and N-sieves, which satisfies causality and edge localization properties. However, his operator relies only on the size of the features and completely ignores the shape. On the other hand, morphological multiscale opening (closing) by reconstruction [18,31], as defined below, considers both shape and size, and satisfies those properties.

Geodesic dilation of size one, i.e. the smallest size in discrete domain, is defined as the minimum of the dilation of the original function g with an SE X of size one and a reference function ρ and is denoted by $\delta_X^1(g,\rho)$. Hence

$$\delta_X^1(g,\rho) = \min(g \oplus X, \rho). \tag{6}$$

Similarly, geodesic erosion of size one is defined as the maximum of the erosion of the original function g with an SE X of size one and a reference function ρ and is denoted by $\varepsilon_X^1(g,\rho)$. Hence

$$\varepsilon_X^1(g,\rho) = \max(g \ominus X, \rho). \tag{7}$$

Now geodesic dilation and erosion of size larger than one may be defined as

$$\delta_X^i(g,\rho) = \min(\delta_X^{(i-1)}(g,\rho) \oplus X, \rho), \tag{8}$$

$$\varepsilon_X^i(g,\rho) = \max(\varepsilon_X^{(i-1)}(g,\rho) \ominus X, \rho) \tag{9}$$

for $i = 1,2,3,\ldots$. Conceptually this may continue indefinitely, but for all practical purposes iteration is terminated at an integer n such that $\delta_X^n(g,\rho) = \delta_X^{(n-1)}(g,\rho)$ and, similarly, when $\varepsilon_X^n(g,\rho) = \varepsilon_X^{(n-1)}(g,\rho)$, because no change would occur after that. Let us call this stable output *reconstruction by dilation* and denote it by $\delta^{(\mathrm{rec})}(g,\rho)$, i.e.,

$$\delta^{(\mathrm{rec})}(g,\rho) = \delta_X^n(g,\rho)$$

and, similarly, we have *reconstruction by erosion* denoted by $\varepsilon^{(\mathrm{rec})}(g,\rho)$, i.e.,

$$\varepsilon^{(\mathrm{rec})}(g,\rho) = \varepsilon_X^n(g,\rho).$$

Based on this operation, *opening by reconstruction of opening* or, simply, *opening by reconstruction* denoted by $g\bar{\circ}B$ may be defined as

$$g\bar{\circ}B = \delta^{(\mathrm{rec})}(g \circ B, g) \tag{10}$$

and *closing by reconstruction* denoted by $g\bar{\bullet}B$ may be defined as

$$g\bar{\bullet}B = \varepsilon^{(\mathrm{rec})}(g \bullet B, g). \tag{11}$$

Therefore, the 'opening by reconstruction' can reconstruct the whole feature through geodesic dilation if at least a part of it can contain the SE. Thus the basic difference between conventional opening and opening by reconstruction is as follows: Conventional opening removes the parts of the bright features or objects that do not fit in the SE, whereas opening by reconstruction either removes the features completely or retains the whole of it. The situation is evident in the example shown in Fig. 1 generated following Pizer [20]. Similar analysis holds for 'closing by reconstruction' in case of dark features. As a result, problems like introduction of new edges and edge displacement do not arise in the case of opening by reconstruction and closing by reconstruction. Hence, a multiscale system designed with these operators satisfies causality and edge localization properties. However, it should be noted that conventional opening and closing operations are far more efficient in removing noise than opening by reconstruction and closing by reconstruction, respectively.

If these operators, i.e., opening and closing by reconstruction, are used with multiscale SEs, the output image should contain only features of that scale and

higher. The difference between the outputs at successive scales then contains features of a particular scale only. In essence, in the difference image the features which can contain the SE at that scale are present completely and others are removed. Thus, the system can be termed as *scale calibrated*. Another property desirable for any filter, known as rotation invariance property, is satisfied by these systems because of use of a disk SE which is isotropic up to the accuracy attainable in discrete domain.

In the following discussion, unless otherwise mentioned, 'open' means 'open by reconstruction' and 'close' means 'close by reconstruction', and consequently '$\circ$' stands for '$\bar{\circ}$' and '$\bullet$' stands for '$\bar{\bullet}$'.

3. Proposed method

3.1. Noise smoothing using multiscale morphology

The noise smoothing technique using multiscale morphology proposed here makes use of weighted averaging of a sequence of morphologically filtered images stacked in different layers of morphological towers [26] as depicted in Fig. 4. In general the presence of noise over a region in an image is manifested in terms of abrupt variation in the intensity as compared to the relatively smoother variation of the desired signal and consequently the edges. This key feature helps us discriminate noise from the image data. However, features of smaller size are affected more as compared to that of larger size. Hence, features of various sizes must be separated out prior to the application of any technique for reducing the noise.

In morphological filtering a bright top-hat transformation [24] extracts bright objects of size smaller than the size of the structuring element present in image as given by the following equation:

$$g_{\text{top}}(r,c) = g(r,c) - (g \circ B)(r,c), \tag{12}$$

where $(g \circ B)(r,c)$ is opening by reconstruction of gray-level image $g(r,c)$ by a disk structuring element B and $i = 1, 2, \ldots, n$ is an integer representing the scale of the structuring element.

The bright top-hat image resulting after filtering by a SE of size i contains all bright features along with noise that are smaller than i. In this sense the bright top-hat transformation is scale calibrated. Also, using the following equation the original image may be recovered as follows.

$$g(r,c) = (g \circ iB)(r,c) + (g(r,c) - (g \circ iB)(r,c)). \tag{13}$$

Modifying Eq. (13) with a notion of multiscale filtering we get

$$\begin{aligned} g(r,c) = {} & (g \circ nB)(r,c) + ((g \circ (n-1)B)(r,c) \\ & -(g \circ nB)(r,c)) + ((g \circ (n-2)B)(r,c) \\ & -(g \circ (n-1)B)(r,c)) + \cdots + (g(r,c) \\ & -(g \circ B)(r,c)) \end{aligned} \tag{14}$$

or,

$$\begin{aligned} g(r,c) = {} & (g \circ nB)(r,c) + F^{\text{o}}_{B}(r,c) \\ & + F^{\text{o}}_{2B}(r,c) + \cdots + F^{\text{o}}_{nB}(r,c), \end{aligned} \tag{15}$$

where

$$F^{\text{o}}_{iB}(r,c) = (g \circ (i-1)B)(r,c) - (g \circ iB)(r,c). \tag{16}$$

Similarly a dark top-hat or a *bottom-hat* image resulting after filtering by an SE of size i contains all dark image features along with noise that are smaller than i. In this sense dark top-hat transformation is, too, scale calibrated. Proceeding in the similar way, we have

$$\begin{aligned} g(r,c) = {} & (g \bullet nB)(r,c) - F^{c}_{B}(r,c) \\ & - F^{c}_{2B}(r,c) - \cdots - F^{c}_{nB}(r,c), \end{aligned} \tag{17}$$

where

$$F^{c}_{iB}(r,c) = (g \bullet iB)(r,c) - (g \bullet (i-1)B)(r,c). \tag{18}$$

Adding Eq. (15) and Eq. (17) and dividing the result by 2 we get

$$\begin{aligned} g(r,c) = {} & \tfrac{1}{2}\{(g \circ nB)(r,c) + (g \bullet nB)(r,c)\} \\ & + \underbrace{\tfrac{1}{2}\Sigma_1^n F^{\text{o}}_{iB}}_{\text{part1}} - \underbrace{\tfrac{1}{2}\Sigma_1^n F^{c}_{iB}}_{\text{part2}}. \end{aligned} \tag{19}$$

Each $(F^{\text{o}}_{iB})(r,c)$ in part1 of Eq. (19) represents the image consisting of bright features at scale i present in the input noisy image. Similarly, each $(F^{c}_{iB})(r,c)$ in part2 represents the image consisting of dark features

at scale i present in the input noisy image. In the reconstruction process equal emphasis is given to each of these feature images through equal weights (which is 1) as suggested by Eq. (19). However, according to our assumption the effect of noise is more in the lower scales. That means noise dominates in the feature images of Eq. (19). So, it is expected that the effect of noise in the reconstructed image gets reduced if we reconstruct the image by giving weights less than one to the feature images. With such views we can modify Eq. (19) to obtain a smooth image as given below.

$$\tilde{g}(r,c) = \tfrac{1}{2}\{(g \circ nB)(r,c) + (g \bullet nB)(r,c)\} + \underbrace{\tfrac{1}{2}\Sigma_1^n k_i^o F_{iB}^o}_{\text{part1}} - \underbrace{\tfrac{1}{2}\Sigma_1^n k_i^c F_{iB}^c}_{\text{part2}}, \tag{20}$$

where $0 \leqslant k_i^o < 1$ and $0 \leqslant k_i^c < 1$.

Now the problem is to estimate the values of the parameters k_i^os and k_i^cs. One simple way of estimating these parameters is to maximize some *goodness* criterion measured on the smooth image. The noise smoothing algorithm generally aims at reducing the abrupt changes and to maintain gradual changes (if any) in the intensity surface of the image. The abrupt changes in the intensity surface profile is manifested in terms of *edginess*. Based on this we consider the Euclidean norm of *Laplacian* of the smooth image as a suitable goodness criterion to be minimized. However, minimization of such type of objective function without any constraint usually leads to trivial solutions. So we need to incorporate certain constraint in the objective function to be minimized. Suppose, the image is corrupted by additive noise as given by

$$g(r,c) = f(r,c) + \eta(r,c).$$

In that case $\sum_r \sum_c (g(r,c) - \tilde{g}(r,c))^2 = \sum_r \sum_c \eta^2(r,c) = N(\mu_\eta^2 + \sigma_\eta^2)$ could be used as the constraint, where μ_η and σ_η are the mean and the variance of noise term, respectively and N is the number of pixels in the image. Thus the objective function to be minimized takes the form

$$E(k_1^o, k_1^c, \ldots, k_n^o, k_n^c) = \sum_r \sum_c \{\nabla^2 \tilde{g}(r,c)\}^2 + \alpha \left\{ \sum_r \sum_c (g(r,c) - \tilde{g}(r,c))^2 - N(\mu_\eta^2 + \sigma_\eta^2) \right\}, \tag{21}$$

where, α is the *Lagrange multiplier*, and $0 \leqslant k_i^o < 1$ and $0 \leqslant k_i^c < 1$. Differentiating Eq. (21) with respect to the parameters $k_1^o, k_1^c, \ldots, k_n^o$ and k_n^c and equating them to zero, we get $2n$ number of simultaneous equations. Solving them we get

$$\begin{pmatrix} k_1^o \\ k_2^o \\ \cdots \\ \cdots \\ k_n^o \\ k_1^c \\ k_2^c \\ \cdots \\ \cdots \\ k_n^c \end{pmatrix} = 2\mathbf{X}^{-1} \begin{pmatrix} \alpha(\overline{gF_1^o}) & -\alpha(\overline{AF_1^o}) & -(\overline{L_A L_1^o}) \\ \alpha(\overline{gF_2^o}) & -\alpha(\overline{AF_2^o}) & -(\overline{L_A L_2^o}) \\ & \cdots & \\ & \cdots & \\ \alpha(\overline{gF_n^o}) & -\alpha(\overline{AF_n^o}) & -(\overline{L_A L_n^o}) \\ \alpha(\overline{gF_1^c}) & -\alpha(\overline{AF_1^c}) & -(\overline{L_A L_1^c}) \\ \alpha(\overline{gF_2^c}) & -\alpha(\overline{AF_2^c}) & -(\overline{L_A L_2^c}) \\ & \cdots & \\ & \cdots & \\ \alpha(\overline{gF_n^c}) & -\alpha(\overline{AF_n^c}) & -(\overline{L_A L_n^c}) \end{pmatrix}, \tag{22}$$

where

$$\mathbf{X} = \begin{pmatrix} (\overline{L_1^o L_1^o} + \alpha\overline{F_1^o F_1^o}) & (\overline{L_1^o L_2^o} + \alpha\overline{F_1^o F_2^o}) & \cdots & (\overline{L_1^o L_n^o} + \alpha\overline{F_1^o F_n^o}) & -(\overline{L_1^o L_1^c} + \alpha\overline{F_1^o F_1^c}) & -(\overline{L_1^o L_2^c} + \alpha\overline{F_1^o F_2^c}) & \cdots & -(\overline{L_1^o L_n^c} + \alpha\overline{F_1^o F_n^c}) \\ (\overline{L_2^o L_1^o} + \alpha\overline{F_2^o F_1^o}) & (\overline{L_2^o L_2^o} + \alpha\overline{F_2^o F_2^o}) & \cdots & (\overline{L_2^o L_n^o} + \alpha\overline{F_2^o F_n^o}) & -(\overline{L_2^o L_1^c} + \alpha\overline{F_2^o F_1^c}) & -(\overline{L_2^o L_2^c} + \alpha\overline{F_2^o F_2^c}) & \cdots & -(\overline{L_2^o L_n^c} + \alpha\overline{F_2^o F_n^c}) \\ \cdots & \cdots & \cdots & \cdots & \cdots & \cdots & \cdots & \cdots \\ \cdots & \cdots & \cdots & \cdots & \cdots & \cdots & \cdots & \cdots \\ (\overline{L_n^o L_1^o} + \alpha\overline{F_n^o F_1^o}) & (\overline{L_n^o L_2^o} + \alpha\overline{F_n^o F_2^o}) & \cdots & (\overline{L_n^o L_n^o} + \alpha\overline{F_n^o F_n^o}) & -(\overline{L_n^o L_1^c} + \alpha\overline{F_n^o F_1^c}) & -(\overline{L_n^o L_2^c} + \alpha\overline{F_n^o F_2^c}) & \cdots & -(\overline{L_n^o L_n^c} + \alpha\overline{F_n^o F_n^c}) \\ (\overline{L_1^c L_1^o} + \alpha\overline{F_1^c F_1^o}) & (\overline{L_1^c L_2^o} + \alpha\overline{F_1^c F_2^o}) & \cdots & (\overline{L_1^c L_n^o} + \alpha\overline{F_1^c F_n^o}) & -(\overline{L_1^c L_1^d} + \alpha\overline{F_1^c F_1^d}) & -(\overline{L_1^c L_2^d} + \alpha\overline{F_1^c F_2^c}) & \cdots & -(\overline{L_1^c L_n^c} + \alpha\overline{F_1^c F_n^c}) \\ (\overline{L_2^c L_1^o} + \alpha\overline{F_2^c F_1^o}) & (\overline{L_2^c L_2^o} + \alpha\overline{F_2^c F_2^o}) & \cdots & (\overline{L_2^c L_n^o} + \alpha\overline{F_2^c F_n^o}) & -(\overline{L_2^c L_1^c} + \alpha\overline{F_2^c F_1^c}) & -(\overline{L_2^c L_2^c} + \alpha\overline{F_2^c F_2^c}) & \cdots & -(\overline{L_2^c L_n^c} + \alpha\overline{F_2^c F_n^c}) \\ \cdots & \cdots & \cdots & \cdots & \cdots & \cdots & \cdots & \cdots \\ \cdots & \cdots & \cdots & \cdots & \cdots & \cdots & \cdots & \cdots \\ (\overline{L_n^c L_1^o} + \alpha\overline{F_n^c F_1^o}) & (\overline{L_n^c L_2^o} + \alpha\overline{F_n^c F_2^o}) & \cdots & (\overline{L_n^c L_n^o} + \alpha\overline{F_n^c F_n^o}) & -(\overline{L_n^c L_1^c} + \alpha\overline{F_n^c F_1^c}) & -(\overline{L_n^c L_2^c} + \alpha\overline{F_n^c F_2^c}) & \cdots & -(\overline{L_n^c L_n^c} + \alpha\overline{F_n^c F_n^c}) \end{pmatrix}$$

Table 1
An example of estimated values of the parameters

Scale	Type of feature			
	Bright feature		Dark feature	
	Parameter	Value	Parameter	Value
1	k_1^o	0.003480940	k_1^c	0.007203650
2	k_2^o	0.012613741	k_2^c	0.018714545
3	k_3^o	0.065167400	k_3^c	0.039894422
4	k_4^o	0.072803162	k_4^c	0.058386658

and

$$A(r,c) = \tfrac{1}{2}\{(g \circ nB)(r,c) + (g \bullet nB)(r,c)\},$$

$$L_i^o(r,c) = \nabla^2 F_i^o(r,c),$$

$$L_i^c(r,c) = \nabla^2 F_i^c(r,c),$$

$$L_A(r,c) = \nabla^2 A(r,c),$$

$$\overline{L_i^o L_j^c} = \frac{1}{(ht * wd)} \Sigma_{r=1}^{ht} \Sigma_{c=1}^{wd} L_i^o(r,c) L_i^c(r,c),$$

$$\overline{F_i^o F_j^c} = \frac{1}{(ht * wd)} \Sigma_{r=1}^{ht} \Sigma_{c=1}^{wd} F_i^o(r,c) F_i^c(r,c),$$

$$\overline{AF_j^o} = \frac{1}{(ht * wd)} \Sigma_{r=1}^{ht} \Sigma_{c=1}^{wd} AF_i^o(r,c),$$

$$\overline{AF_j^c} = \frac{1}{(ht * wd)} \Sigma_{r=1}^{ht} \Sigma_{c=1}^{wd} AF_i^c(r,c),$$

$$\overline{gF_j^o} = \frac{1}{(ht * wd)} \Sigma_{r=1}^{ht} \Sigma_{c=1}^{wd} gF_i^o(r,c),$$

$$\overline{gF_j^c} = \frac{1}{(ht * wd)} \Sigma_{r=1}^{ht} \Sigma_{c=1}^{wd} gF_i^c(r,c),$$

$$\overline{L_A L_j^o} = \frac{1}{(ht * wd)} \Sigma_{r=1}^{ht} \Sigma_{c=1}^{wd} L_A(r,c) L_i^o(r,c), \quad \text{and}$$

$$\overline{L_A L_j^c} = \frac{1}{(ht * wd)} \Sigma_{r=1}^{ht} \Sigma_{c=1}^{wd} L_A(r,c) L_i^c(r,c).$$

Value of α is chosen iteratively so as to satisfy the given constraint [5,13,29]. The experiment has been carried out on quite a few images corrupted with various types of noise; however, for the sake of presentation, we have taken an example image along with its Gaussian noise corrupted version. The values estimated are shown in Table 1. Fig. 2 shows the noise corrupted version and the noise grains present in it at different scales. The parameter values follow an increasing order, i.e., $k_1^o \leqslant k_2^o \leqslant k_3^o \cdots \leqslant k_n^o$ and $k_1^c \leqslant k_2^c \leqslant k_3^c \cdots \leqslant k_n^c$, which conform with the observation that introduction of random noise, in general, generates perturbation at lower scales [38].

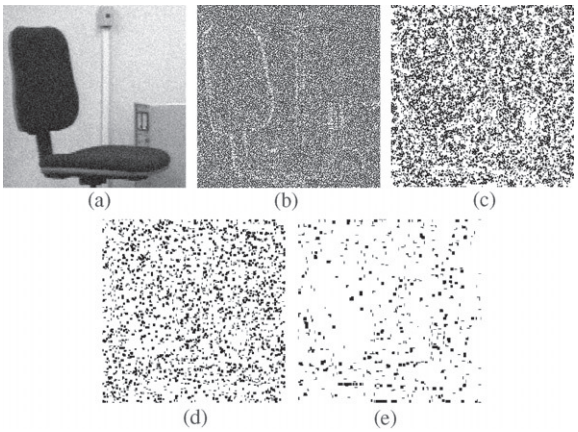

Fig. 2. Illustrates Gaussian noise grains at different scales: (a) noisy image, (b) scale 1, (c) scale 2, (d) scale 3, and (e) scale 4.

However, estimation of the parameters incurs a huge computational cost. To avoid such huge computational cost and also to use fixed point arithmetic operations (for further speed up of the algorithm), we have chosen $k_n^o = k_n^c = \frac{1}{2}$, $k_{i-1}^o = \frac{1}{2} k_i^o$ and $k_{i-1}^c = \frac{1}{2} k_i^c$ for $i = n, n-1, \ldots$. However, these weights are set heuristically guided by the experimental results. Therefore this algorithm is suitable for a class of images that satisfy the monotonies of the noise contents with scale. The efficacy of this selection is established in Section 4.

This selection leads to

$$\tilde{g}(r,c)=\frac{1}{2}\{(g\circ nB)(r,c)+(g\bullet nB)(r,c)\}$$
$$+\frac{1}{2}\frac{\dfrac{\dfrac{\frac{1}{2}F_1^{o}+F_2^{o}}{2}+F_3^{o}}{2}+F_4^{o}}{2}+\cdots}{\vdots}}{2}+F_n^{o}}{2}$$
$$-\frac{1}{2}\frac{\dfrac{\dfrac{\frac{1}{2}F_1^{c}+F_2^{c}}{2}+F_3^{c}}{2}+F_4^{c}}{2}+\cdots}{\vdots}}{2}+F_n^{c}}{2}. \tag{23}$$

Let us define

$$g_{av_1}^{o}(r,c)=\tfrac{1}{2}\{F_B^{o}(r,c)\} \tag{24}$$

$$g_{av_i}^{o}(r,c)=\tfrac{1}{2}\{g_{av(i-1)}^{o}(r,c)+F_{iB}^{o}\} \tag{25}$$

$$g_{av_1}^{c}(r,c)=\tfrac{1}{2}\{F_B^{c}(r,c)\} \tag{26}$$

$$g_{av_i}^{c}(r,c)=\tfrac{1}{2}\{g_{av(i-1)}^{c}(r,c)+F_{iB}^{c}\} \tag{27}$$

and

$$\bar{g}(r,c)=\tfrac{1}{2}\{(g\circ nB)(r,c)+(g\bullet nB)(r,c)\}. \tag{28}$$

Then Eq. (23) can be rewritten as

$$\tilde{g}(r,c)=\bar{g}(r,c)+\tfrac{1}{2}g_{av_n}^{o}(r,c)-\tfrac{1}{2}g_{av_n}^{c}(r,c). \tag{29}$$

Eq. (29) can be implemented on morphological towers as described elaborately in the next subsection.

In the proposed scheme the scale specific feature images are extracted using top-hat transformation based on multiscale opening by reconstruction and closing by reconstruction. There exist other methods for extracting scale specific features from images which use median filter [2], stack filter [22], alternate sequential filter [32,39], M- and N-sieves [3,16]. Second, we have reconstructed the image from the decomposed ones by their linear combination. However, non-linear combinations are also employed for the purpose; for example, Toet [38] used max operator to reconstruct the image from morphological tree.

3.2. A simple illustration in one dimension

A simplified illustration of the proposed scheme applied to one-dimensional signal is shown in Fig. 3 for easy understanding. The function $f(t)$ has salient features manifested as *crests* and *troughs* of different height (or depth) and width located at different positions. The noise in the function is manifested in terms of the narrow peaks and troughs at different positions. Our objective is to smooth the noise of the function $g(t)$. The line segment L of unit length and its higher order dilates kL (where $k=1,2,3$) are used as structuring elements (SE) for extracting the salient features at different scales from the function as described below.

- The opening operation with the SE kL removes the crests which are narrower than the width k while the closing operation fills up the troughs narrower than the width k.
- The function $F_k^{o}(t)=(g\circ(k-1)L)(t)-(g\circ kL)(t)$ contains only the crests of width smaller than k but larger than $(k-1)$ and the function $F_k^{c}(t)=(g\bullet kL)(t)-(g\bullet(k-1)L)(t)$ contains only the troughs of width smaller than k but larger than $(k-1)$. Proceeding in this way we construct the function $F_1^{o}(t),F_2^{o}(t),F_3^{o}(t)$ and $F_1^{c}(t),F_2^{c}(t),F_3^{c}(t)$ (see Fig. 3).
- We take recursive averaging of the functions obtained in the previous steps. We first construct the function $g_{\mathrm{av1}}^{o}(t)=\frac{1}{2}[F_1^{o}(t)]$, then the functions $g_{\mathrm{av2}}^{o}(t)=\frac{1}{2}[g_{\mathrm{av1}}^{o}+F_2^{o}(t)]$ and $g_{\mathrm{av3}}^{o}(t)=\frac{1}{2}[g_{\mathrm{av2}}^{o}+F_3^{o}(t)]$, respectively. In a similar way the function $g_{\mathrm{av3}}^{c}(t)$ is constructed.
- The function $\bar{g}(t)$ is obtained by averaging $(g\circ 3L)(t)$ and $(g\bullet 3L)(t)$.
- The smoothed function is then formed by combining the functions $\bar{g}(t)$, $g_{\mathrm{av3}}^{o}(t)$ and $g_{\mathrm{av3}}^{c}(t)$ as shown below:

$$\tilde{g}(t)=\bar{g}(t)+\tfrac{1}{2}g_{\mathrm{av3}}^{o}(t)-\tfrac{1}{2}g_{\mathrm{av3}}^{c}(t). \tag{30}$$

Comparing $\tilde{g}(t)$ with $f(t)$ at each sample point t it is readily seen that the height (depth) of the crests (troughs) have decreased but disproportionately. The change in height is more for crests of narrower width. This is true for crests also. This would not be possible using mean filtering. The smooth function is found to be less affected by noise spikes without any noticeable

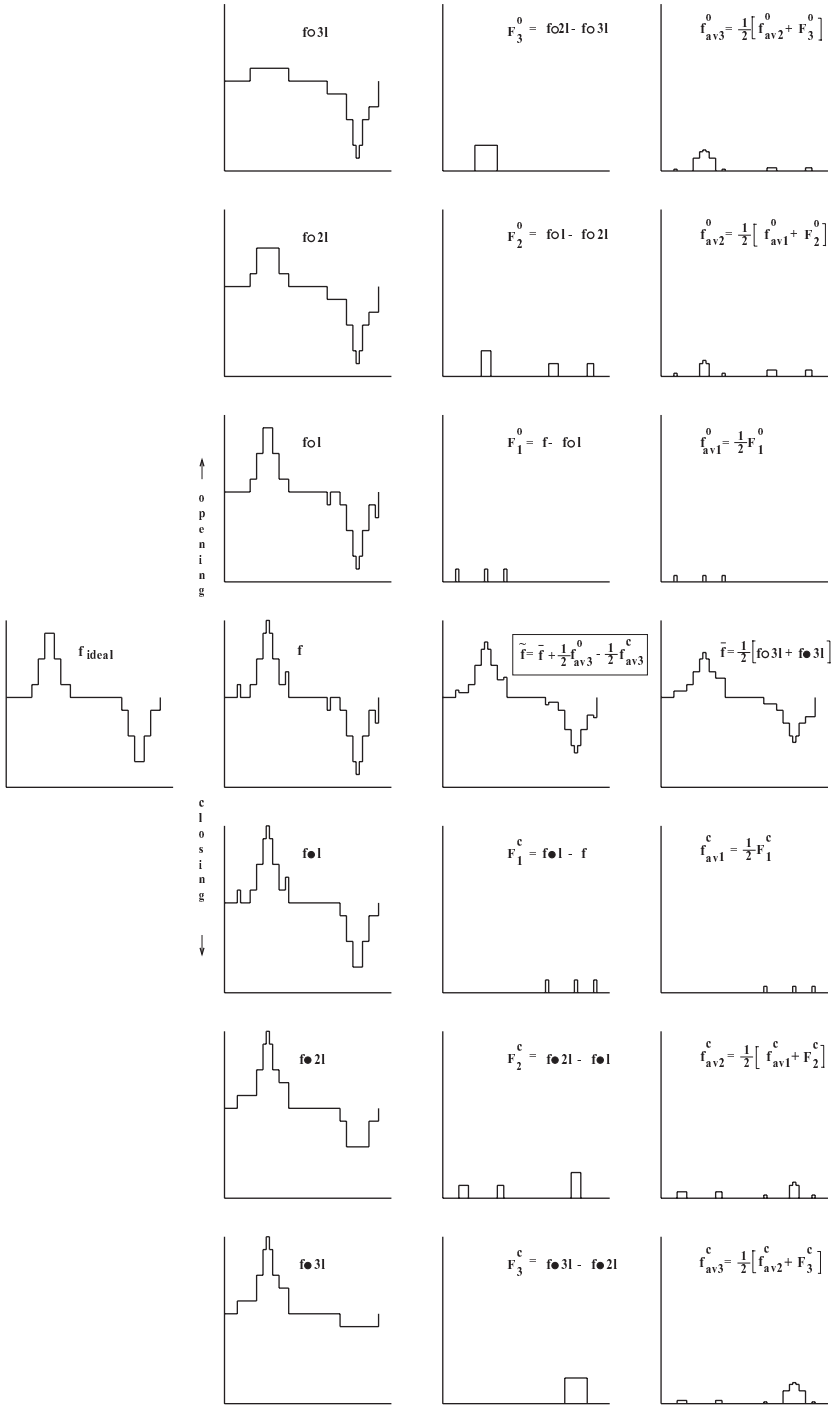

Fig. 3. Multiscale morphological noise smoothing of a function.

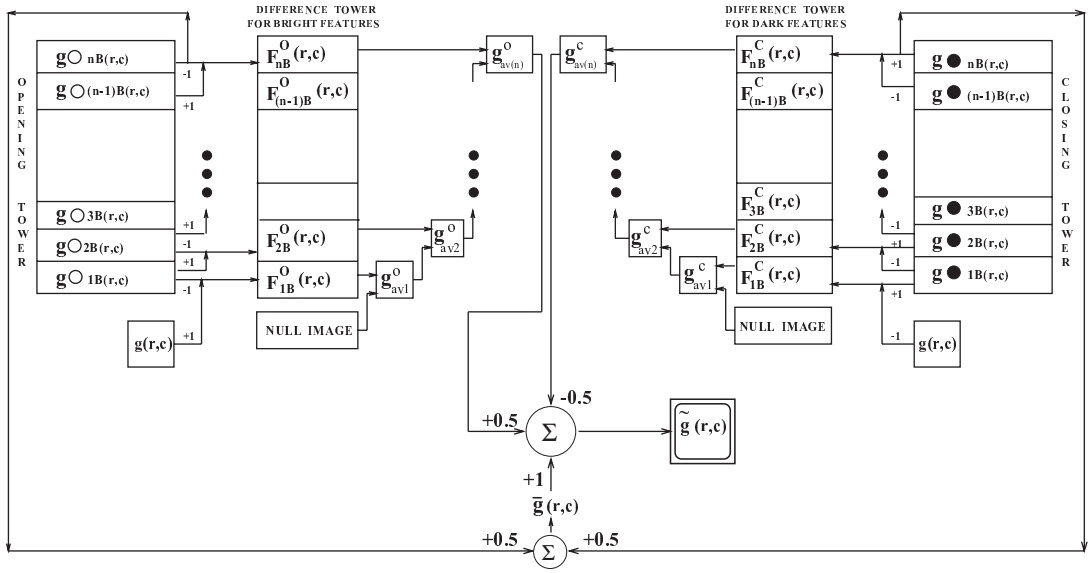

Fig. 4. Noise smoothing scheme using morphological towers.

change in sharpness and location of valid edges. The scheme explained for this one-dimensional case may as well be extended to two dimension as described below.

3.3. Implementation

The implementation of Eq. (29) describing feature based noise smoothing scheme involves construction of a number of morphological towers.

3.3.1. Construction of morphological towers

The noisy image to be smoothed is made to undergo a sequence of gray-scale morphological opening by reconstruction with a disc structuring element and its higher order homothetics. The resulting sequence of images is kept in a stack called the *opening tower* as shown in Fig. 4. An identical tower, called closing tower, is constructed with the sequence of the images resulted from multiscale closing by reconstruction of the input noisy image. Therefore, the ith entry in the opening (closing) tower contains the image opened (closed) with the structuring element iB as given below.

$$(g \circ iB)(r,c) = ((g \ominus iB) \oplus iB)(r,c) \tag{31}$$

$$(g \bullet iB)(r,c) = ((g \oplus iB) \ominus iB)(r,c) \tag{32}$$

for $i = 1, 2, \ldots, n$.

3.3.2. Construction of difference towers

As stated earlier the image resulting after morphological opening using a structuring element iB contains only those features of the original image that are equal to or larger than the size of the structuring element iB. Likewise the image resulting after a morphological opening using a structuring element $(i+1)B$ contains all those features of the original image that are equal to or larger than the size of the structuring element $(i+1)B$. Thus a difference of these two images gives rise to another image which contains only those features of the original image that have size greater than or equal to that of iB but less than that of $(i+1)B$. This holds good for the multiscale closings of the images also.

Accordingly, two difference towers for opening and closing are constructed by carrying out difference operations between all successive pairs of images resulting after morphological opening (closing) operations. Fig. 4 shows two such *difference towers*. Thus the ith layer of the difference tower corresponding to bright and dark features contain the images obtained by

following operations.

$$F^{o}_{iB}(r,c) = (g \circ (i-1)B)(r,c) - (g \circ iB)(r,c), \quad (33)$$

$$F^{c}_{iB}(r,c) = (g \bullet iB)(r,c) - (g \bullet (i-1)B)(r,c) \quad (34)$$

for $i = 1, 2, \ldots, n$.

3.3.3. Construction of smooth image

- A recursive averaging of the images stacked in difference tower corresponding to opening (closing) is carried out. We start with a null image and select the image at the lowest layer of the difference tower and form another image by averaging them. Then the average of the resulting image and the image in the next higher layer of the corresponding difference tower is computed to form another image. This is continued until the top of the tower is reached. This is described mathematically by Eqs. (24)–(27).
- The average of the images resulting after opening and closing of the input image by the largest homothetic of the SE is also computed as described by Eq. (28). Note that the average, everywhere, denotes pixel-wise average of images.
- Finally, the smooth image is obtained by combining three images as given by

$$\tilde{g}(r,c) = \bar{g}(r,c) + \tfrac{1}{2} g^{o}_{\mathrm{av}_n}(r,c) - \tfrac{1}{2} g^{c}_{\mathrm{av}_n}(r,c). \quad (35)$$

The '+' and '−' operations are applied on corresponding pixels of three different images.

4. Experimental results and discussion

The proposed algorithm has been tested on several images. However, the results are shown here for a single image corrupted with different kinds of noise as shown in Fig. 5 [1(a)–7(a)]. Various kinds of noise considered in the experiment include *exponential*, *Gaussian*, *Poisson*, *Rayleigh*, *shot*, *uniform* and *speckle* noise — the details of which are listed in Table 2. For generating noise we made use of image processing software *Khoros210*. The results of proposed algorithm are shown in Fig. 5 [1(b)–7(b)]. We have compared our results with those of *median filter* (see Fig. 5 [1(c)–7(c)]). *Crimmins filter* (see Fig. 5 [1(d)–7(d)]), and *Anisotropic diffusion smoothing* [27,42] (see Fig. 5[1(e)–7(e)]). In the experiment we have chosen $n = 6$ for our proposed method. For median filter and Crimmins filter the mask size used is 7×7. For anisotropic diffusion smoothing the value of $\delta t, \lambda$ and number of iterations are taken as 0.5, 1.0 and 20, respectively. The values of all these parameters are chosen to obtain visually optimum results.

Qualitative evaluation (by human observer) reveals that median filter has more or less blurred the thin features of the image. Results of Crimmins filter are better than those of median filter and it has proved to be the best for smoothing speckle noise. Results of the proposed method show relatively less blurring of thin features with appreciable noise cleaning and it has greatly outperformed other methods in smoothing shot noise. However, the proposed method has higher space complexity as compared to others. Considering overall performance it can be said in essence, that the proposed multiscale morphological technique is a good edge-preserving smoothing technique. For quantitative comparison of performances of the methods referred here we have studied the followings measures.

4.1. Signal-to-noise ratio

Suppose $I(r,c)$ and $I_{\mathrm{n}}(r,c)$ denote noise-free and noisy image of the same scene. Signal-to-noise ratio (SNR) is defined as the ratio of signal power to the noise power as given below.

$$\mathrm{SNR} = \frac{\Sigma_r \Sigma_c I^2(r,c)}{\Sigma_r \Sigma_c \{I(r,c) - I_{\mathrm{n}}(r,c)\}^2}. \quad (36)$$

The more the value of SNR the better is the noise smoothing method. It may be measured as ratio or in terms of dB. In Table 3 we have presented SNR values (as ratio) of the smooth images resulting from various methods. We also have ranked the methods depending on the SNR values. Higher relative score is assigned to better method. From Table 3 it is evident that the total score of our proposed method is the second highest among all other methods. In most of the cases the SNR value is either the highest or the second highest.

4.2. Mean busyness

Busyness profile of an image gives an idea of spatial variation in intensity. Mean busyness value is an average of busyness values of all the pixels in the

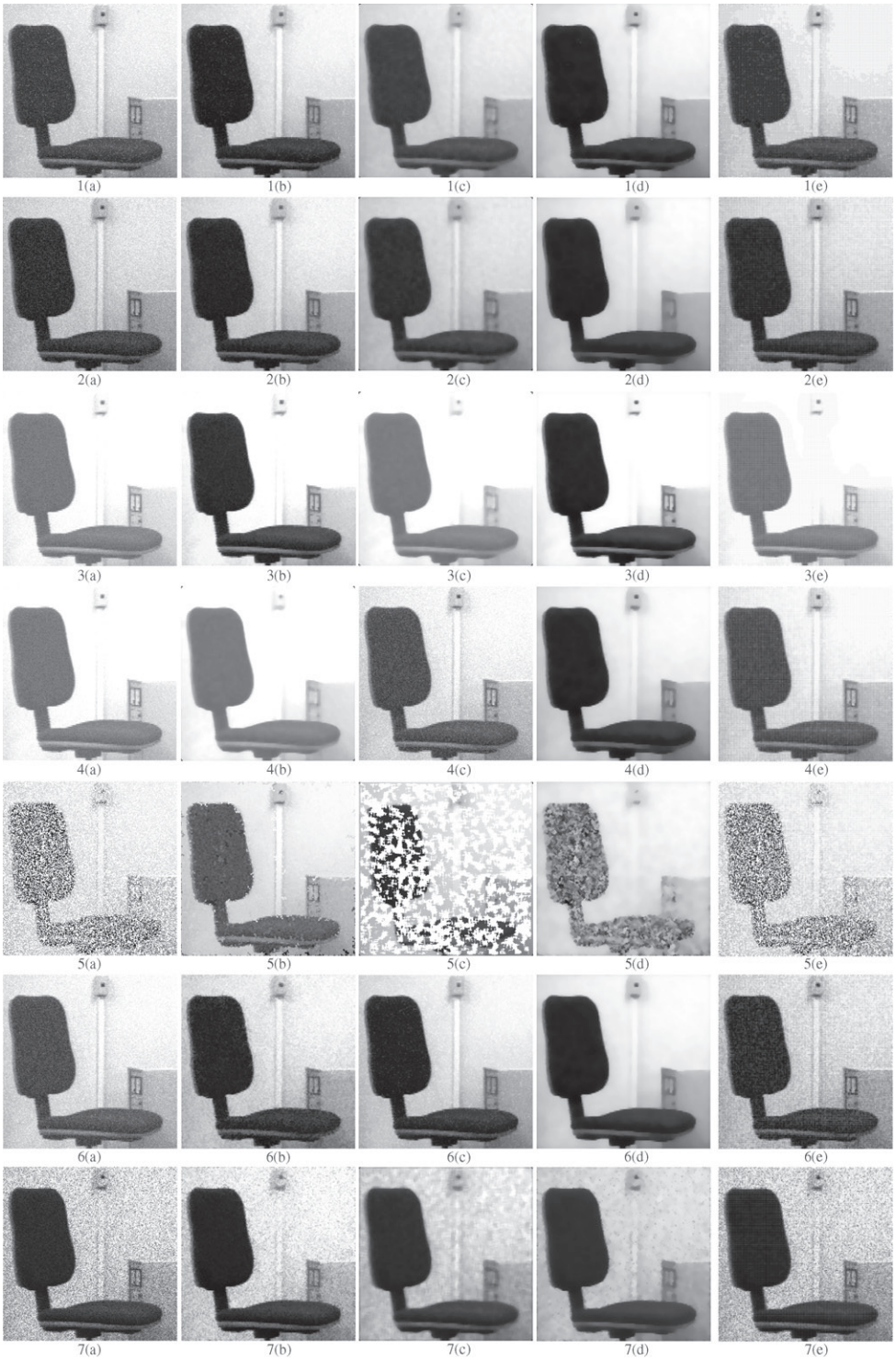

Fig. 5. (a) Original noisy image; (b) result of proposed multiscale morphological noise removal filtering; (c) result of median filtering; (d) result of *Crimmins* algorithm; (e) results of anisotropic diffusion smoothing. (1) *Exponential* noise; (2) *Gaussian* noise; (3) *Poisson* noise; (4) *Rayleigh* noise; (5) *shot* noise; (6) *uniform* noise; (7) *speckle* noise.

Table 2
Different types of noise and their parameters used in the experiment

Fig. no.	Type of noise	Parameter attributes	Values of the parameters	Whether additive or multiplicative
1(a)	Exponential	Variance	255.0	Additive
2(a)	Gaussian	Mean Variance	0.0 255.0	Additive
3(a)	Poisson	Amount of time Variance	2000 75.0	Additive
4(a)	Rayleigh	Variance	255.0	Additive
5(a)	Shot	Percentage of spikes Real value of spike Imaginary value of spike	70 255.0 0.0	Additive
6(a)	Uniform	Minimum value Maximum value	−50.0 +50.0	Additive
7(a)	Speckle	Mean Standard deviation	1.0 +0.28	Multiplicative

Table 3
Signal-to-noise ratio (SNR) for different noise removal schemes[a]

Noise type	Input SNR	Signal-to-noise ratio and scores							
		MMS		MF		CA		ADS	
		SNR	Score	SNR	Score	SNR	Score	SNR	Score
Exp	60.695696	107.092369	3	128.374554	4	84.032957	1	101.385678	2
Gus	110.967612	521.394035	2	359.873484	1	554.378836	3	664.503600	4
Pos	6.323838	12.321112	1	13.584419	2	14.199405	4	13.864437	3
Ral	25.231925	30.637288	3	29.966759	2	26.847579	1	30.924575	4
Sht	2.597885	5.025113	4	2.479764	1	3.920223	3	3.184999	2
Uni	35.734041	249.829078	3	178.546900	2	390.640388	4	131.178951	1
Spk	17.507818	101.459861	3	89.792234	2	106.833882	4	30.123955	1
Total			19		14		20		17

[a]Noise type: Exp: Exponential noise, Gus: Gaussian noise, Pos: Poisson noise, Ral: Rayleigh noise, Sht: shot noise, Uni: uniform noise, Spk: speckle noise. MMS: multiscale morphological smoothing, MF: median filtering, CA: Crimmins algorithm, ADS: anisotropic diffusion smoothing.

image. In general, the presence of noise in an image raises the mean busyness value of the image. A noise removal algorithm should reduce this raised mean busyness value and bring it as close to that of the original noise-free image as possible. In this section we have studied the smoothing ability of the algorithms in terms of *deviation in mean busyness* (DMB) values of the noisy images and compared that with other methods.

Wu et al. [43] computed *busyness* at each pixel in an image as the *median* of the absolute vertical and horizontal differences in gray values over a 3×3 mask. The busyness values of all the pixels are then averaged to get the *mean busyness* value of the image. Thus, mean busyness MB is computed as

$$\mathrm{MB}=\frac{1}{N}\Sigma_r\Sigma_c\,\mathrm{Median}\{|d_k(r,c)|\}, \tag{37}$$

where $d_k(r,c)$ is the kth vertical and horizontal difference in a 3×3 mask of the image. Finally, deviation in mean busyness value of a smooth image $\tilde{g}$ is obtained by subtracting the mean busyness value of

Table 4
Deviation in mean busyness value (DMB) for different noise removal schemes[a]

Type of noise	Deviation in mean busyness value and score of the scheme								
	NI	MMS		MF		CA		ADS	
	DMB	DMB	Score	DMB	Score	DMB	Score	DMB	Score
Exp	10.921769	1.776302	1	0.061684	4	−0.663406	3	1.085721	2
Gus	14.009873	2.513388	1	0.228851	4	−0.670080	3	1.416486	2
Pos	3.561615	0.076848	4	−0.519846	2	−0.869204	1	−0.343052	3
Ral	12.423284	1.810181	1	0.213318	4	−0.672295	3	1.106729	2
Sht	56.100977	−0.485336	4	2.166444	3	15.512188	2	35.877724	1
Uni	26.590066	3.531104	2	1.396079	3	−0.540330	4	7.273403	1
Spk	31.357986	5.062269	2	1.696948	3	0.053672	4	14.632311	1
Total			15		23		20		12

[a]Type of noise: Exp: exponential noise, Gus: Gaussian noise, Pos: Poisson noise, Ral: Rayleigh noise, Sht: shot noise, Uni: uniform noise, Spk: speckle noise. NI: noisy image, MMS: multiscale morphological smoothing, MF: median filtering, CA: Crimmins algorithm, ADS: anisotropic diffusion smoothing.

Table 5
Correct processing ratio value CPR for different noise removal schemes[a]

Type of noise	Correct processing ratio value and score of the scheme							
	MMS		MF		CA		ADS	
	CPR	Score	CPR	Score	CPR	Score	CPR	Score
Exp	0.894104	3	0.912628	4	0.883774	2	0.882538	1
Gus	0.922318	3	0.930511	4	0.920120	2	0.902786	1
Pos	0.550140	2	0.636810	3	0.542679	1	0.755737	4
Ral	0.962555	3	0.973022	4	0.908737	1	0.941376	2
Sht	0.509003	4	0.503113	3	0.268234	1	0.501587	2
Uni	0.964340	3	0.970032	4	0.951797	2	0.933578	1
Spk	0.950699	3	0.957886	4	0.939911	2	0.921738	1
Total		21		26		11		12

[a]Type of noise: Exp: exponential noise, Gus: Gaussian noise, Pos: Poisson noise, Ral: Rayleigh noise, Sht: shot noise, Uni: uniform noise, Spk: speckle noise. NI: noisy image, MMS: multiscale morphological smoothing, MF: median filtering, CA: Crimmins algorithm, ADS: anisotropic diffusion smoothing.

the ideal noise-free image from that of the smoothed image (see Eq. (38)).

$$\mathrm{DMB}(\tilde{g}) = \mathrm{MB}(\tilde{g}) - \mathrm{MB}(f). \tag{38}$$

For each kind of noise we have computed the absolute difference between the mean busyness values of the noisy image and the smooth images resulting from different methods. A method is ranked by its score. Lower the magnitude of DMB better is the performance of the smoothing algorithm and higher is the score awarded to it. A negative value of DMB implies the over-smoothing performed by the associated algorithm and it also indicates the loss of certain edge features. Table 4 summarizes the observation. From the table it is evident that the overall (as well as individual) score of the proposed method falls behind those of MF and CA. However, in almost all cases CA has performed over-smoothing.

4.3. Correct processing ratio

A pixel in a smooth image is said to be *noisy* if its gray value is not same as that of the ideal noise-free image. This difference in gray value can be due to some amount of noise still present or due to degradation

of feature. The basic purpose of a noise smoothing algorithm should be to modify the gray value of the noisy pixels keeping those of the noise-free pixels unaltered as far as possible. In this context the *correct processing ratio* CPR is defined as [43]

$$\mathrm{CPR} = \frac{1}{N}\Sigma_r\Sigma_c\{I_B(r,c) + I_C(r,c)\}, \tag{39}$$

where N is the total number of pixels in the image, and $I_B(r,c)$ and $I_C(r,c)$ are defined as

$$I_B(r,c) = \begin{cases} 1 \text{ if } g(r,c) = f(r,c) \text{ and } \tilde{g}(r,c) = g(r,c), \\ 0 \text{ otherwise} \end{cases} \tag{40}$$

and

$$I_C(r,c) = \begin{cases} 1 \text{ if } g(r,c) \neq f(r,c) \text{ and } \tilde{g}(r,c) \neq g(r,c), \\ 0 \text{ otherwise,} \end{cases} \tag{41}$$

where $f(r,c)$, $g(r,c)$ and $\tilde{g}(r,c)$ are, respectively, the ideal noise-free, noisy and the smooth image. A good edge-preserving smoothing algorithm should have CPR value very close to unity. Accordingly, we have given scores to the methods. From the Table 5 it is evident that our proposed method has the second highest ranking in terms of its overall score.

5. Modification of the proposed scheme considering noise statistics: MMS-2

As mentioned earlier that the noise grains are expected to predominate in the lower range of scale. With such view we have assigned progressively lower weightages to the feature images of low scale. However, though it is agreed upon by many researchers (e.g., [3,38]) that random unstructured noise dominate at the lower scale, the way we assign weightages to the feature images during reconstruction is purely ad hoc in nature. On the other hand, estimating the weights through optimization of goodness criterion as

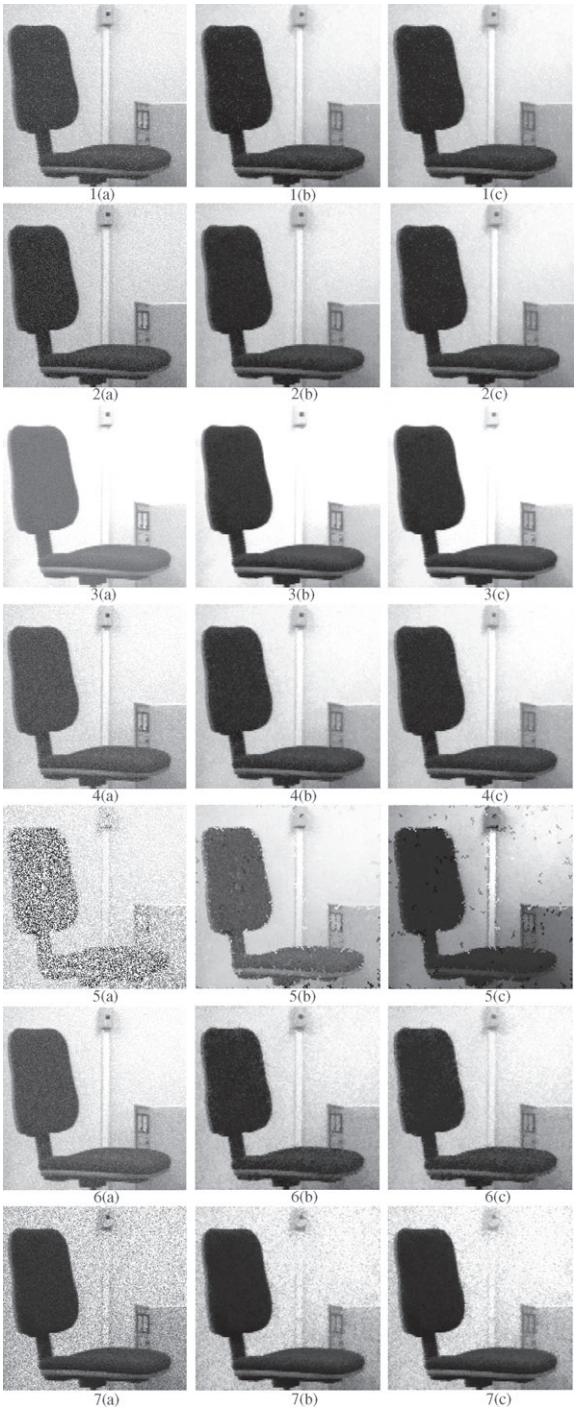

Fig. 6 (a) Original noisy image; (b) result of proposed multiscale morphological noise removal filtering (MMS-1); (c) result of proposed multiscale morphological noise removal filtering using noise statistics (MMS-2). (1) *Exponential* noise; (2) *Gaussian* noise; (3) *Poisson* noise; (4) *Rayleigh* noise; (5) *shot* noise; (6) *uniform* noise; (7) *speckle* noise.

Table 6
Signal-to-noise ratio (SNR) for MMS-1 and MMS-2[a]

Noise type	Input SNR	Signal-to-noise ratio and scores			
		MMS-1		MMS-2	
		SNR	Score	SNR	Score
Exp	60.695696	107.092369	2	106.637728	1
Gus	110.967612	521.394035	1	526.863226	2
Pos	6.323838	12.321112	2	12.008656	1
Ral	25.231925	30.637288	1	30.986411	2
Sht	2.597885	5.025113	1	5.242757	2
Uni	35.734041	249.829078	1	258.817539	2
Spk	17.507818	101.459861	1	106.344694	2
Total			9		12

[a]Noise type: Exp: exponential noise, Gus: Gaussian noise, Pos: Poisson noise, Ral: Rayleigh noise, Sht: shot noise, Uni: uniform noise, Spk: speckle noise. MMS-1: multiscale morphological smoothing, MMS-2: multiscale morphological smoothing using noise statistics.

suggested in Eq. (22) incurs a huge computational cost for each image. A compromise between these two approaches might be assigning weightage depending on the amount of noise present at a scale. Since we have no a priori knowledge of noise statistics at individual scale, we suggest an empirical formula for computing weightages for bright and dark feature images at scale i, respectively, as

$$k_i^{\mathrm{o}} = \frac{\eta_i^{\mathrm{o}}}{\Sigma_{i=0}^{n}\eta_i^{\mathrm{o}}}, \tag{42}$$

$$k_i^{c} = \frac{\eta_i^{c}}{\Sigma_{i=0}^{n}\eta_i^{c}}, \tag{43}$$

where

$$\eta_i^{\mathrm{o}} = \frac{(\text{image size})(\text{size of } iB)}{\sum_r \sum_c F_{iB}^{\mathrm{o}}(r,c)}, \tag{44}$$

$$\eta_i^{c} = \frac{(\text{image size})(\text{size of } iB)}{\sum_r \sum_c F_{iB}^{c}(r,c)} \tag{45}$$

for $i = 1, 2, 3, \ldots, n$. However, if the denominators of Eqs. (44) and (45) are zero, we assign zero value to k_i^{o} and k_i^{c}. Finally, smooth image is reconstructed using Eq. (16). Let us call this scheme MMS-2 and the previous one MMS-1.

We have reconstructed new sets of results following this method and compared these with that of MMS-1 obtained previously. The images resulting after executing MMS-2 on the same set of input noisy images are shown in Fig. 6.

5.1. Comparison between MMS-1 and MMS-2

Qualitative comparison by human observer reveals that the performance of MMS-1 and MMS-2 are almost same. Apart from visual judgment we have compared the SNR, DMB and CPR values of the images resulting from MMS-1 and MMS-2 for each type of noise. The same convention of ranking a method is followed. The measures are summarized in Tables 6–8 as follows.

Table 6 shows the SNR values of the images resulting from MMS-1 and MMS-2 along with the ranks. The SNR values in most cases are found to improve when noise statistics is considered. Table 7 shows the DMB values of the images resulting from MMS-1 and MMS-2 along with the ranks. From the table it is evident that the performances of MMS-1 and MMS-2 in terms of deviation in mean business value are almost same. However, very precisely speaking the overall performance of MMS-1 is slightly better. Again as before, we have computed the CPR values of the images resulting from MMS-1 and MMS-2 and compared them assigning ranks. Table 8 shows the CPR values of the images resulting from MMS-1 and MMS-2 along with the scores. The overall correct processing of MMS-2 is found to be slightly better than that of MMS-1.

Table 7
Deviation in mean busyness values (DMB) for MMS-1 and MMS-2[a]

Type of noise	Deviation in mean busyness value and score of the scheme				
	NI	MMS-1		MMS-2	
	DMB	DMB	Score	DMB	Score
Exp	10.921769	1.776302	2	1.760339	1
Gus	14.009873	2.513388	2	2.580885	1
Pos	3.561615	0.076848	2	0.079354	1
Ral	12.423284	1.810181	2	1.898009	1
Sht	56.100977	−0.485336	2	−0.600246	1
Uni	26.590066	3.531104	1	3.470512	2
Spk	31.357986	5.062269	2	5.118432	1
Total			13		8

[a]Type of noise: Exp: exponential noise, Gus: Gaussian noise, Pos: Poisson noise, Ral: Rayleigh noise, Sht: shot noise, Uni: uniform noise, Spk: speckle noise. NI: Noisy image, MMS-1: multiscale morphological smoothing, MMS-2: multiscale morphological smoothing using noise statistics.

Table 8
Correct processing ratio value (CPR) for MMS-1 and MMS-2[a]

Type of noise	Correct processing ratio value and score of the scheme			
	MMS-1		MMS-2	
	CPR	Score	CPR	Score
Exp	0.894104	1	0.894684	2
Gus	0.922318	2	0.921860	1
Pos	0.550140	2	0.549713	1
Ral	0.962555	2	0.961853	1
Sht	0.509003	1	0.509415	2
Uni	0.964340	1	0.964981	2
Spk	0.950699	1	0.950806	2
Total		10		11

[a]Type of noise: Exp: exponential noise, Gus: Gaussian noise, Pos: Poisson noise, Ral: Rayleigh noise, Sht: shot noise, Uni: uniform noise, Spk: speckle noise. MMS-1: multiscale morphological smoothing, MMS-2: multiscale morphological smoothing using noise statistics.

6. Conclusion

In this paper we present a method for edge preserving smoothing of gray-scale images using multiscale morphology. The method is based on manipulating the intensity of scale-specific features present in the noisy image. The proposed scheme has been illustrated in one dimension. Then it has been implemented using morphological towers to smooth noise in 2-D images. The algorithm has been tested on sample images corrupted with various kinds of noise. The results have been compared with those of other standard methods. A comparative study of performance of various methods have been carried out through some standard performance measures, like signal-to-noise ratio, deviation in mean busyness and correct processing ratio. It is found that the performance of the proposed method is satisfactory and in some cases superior to other methods referred in this paper. The proposed method is then modified considering the noise statistics.

References

[1] G. Agam, H. Luo, I. Dinstein, Morphological approach for dashed line detection, In: R. Kasturi, K. Tombre (Eds.), First International Workshop on Graphics Recognition — Methods and Applications, University Park, PA, USA, Lecture Notes in Computer Science, Vol. 1072, Springer, Berlin, 1995, pp. 92–105.

[2] J.A. Bangham, T.G. Campbell, R.V. Aldridge, Multiscale median and morphological filters for 2D pattern recognition, Signal Processing 38 (1994) 387–415.

[3] J.A. Bangham, R. Harvey, P.D. Ling, R.V. Aldridge, Morphological scale-space preserving transforms in many dimensions, J. Electron. Imaging 5 (3) (July 1996) 283–299.

[4] R.V.D. Boomgaard, L. Dorst, The Morphological Equivalent of Gaussian Scale-Space, in: J. Sporring, M. Nielsen, L. Florack, P. Johansen (Eds.), Gaussian Scale-Space Theory, Vol. 8, Kluwer Academic Press, Netherlands, 1997.

[5] B. Chanda, D. Dutta Majumder, Digital Image Processing and Analysis, Prentice-Hall Pvt. Ltd., New Delhi, 2000.
[6] M. Chen, P. Yan, A multiscaling approach based on morphological filtering, IEEE Trans. Pattern Anal. Mach. Intell. 11 (1989) 694–700.
[7] Chien H. Lin, Chung J. Kuo, Chia H. Yeh, Noise reduction of vq encoded images through anti-gray coding, IEEE Trans. Image Process. 8 (1999) 33–40.
[8] T.R. Crimmins, Geometric filter for speckle reduction, Appl. Opt. (1985) 24.
[9] M. Duff, Parallel processors for digital image processing, in: P. Stucki (Ed.), Advances in Digital Image Processing, Plenum, New York, 1979.
[10] A. Gady, I. Dinstein, Compound regulated morphological operations applied to map analysis, Proceedings of the 3rd IAPR International Workshop on Graphics Recognition, GREC'99, Jaipur, India, September 26–27, 1999, pp. 83–90.
[11] A. Gasteratos, I. Andreadis, Soft mathematical morphology: extensions, algorithms and implementations, in: P.W. Hawkes (Ed.), Advances in Imaging and Electron Physics, Vol. 110, Academic Press, San Diego, California, 1999, pp. 63–99 (Chapter 3).
[12] M.J.E. Golay, Hexagonal parallel pattern transformations, IEEE Trans. Comput. C-18 (1969) 733–740.
[13] R.C. Gonzalez, R.E. Woods, Digital Image Processing, Addison-Wesley, Reading, MA, 1999.
[14] R.M. Haralick, L.G. Shapiro, Computer and Robot Vision, Vol. 1, Addison-Wesley, Reading, MA, 1992.
[15] R.M. Haralick, S.R. Sternberg, Xnnhua Zhuang, Image analysis using mathematical morphology, IEEE Trans. Pattern Anal. Mach. Intell. PAMI-9 (1987) 142–156.
[16] R. Harvey, A. Bosson, J.A. Bangham, A comparison of linear and nonlinear scale-space filters in noise, Signal Processing VIII, 1996, pp. 1777–1781, ISBN 88-86179-83.
[17] J.C. Klein, J. Serra, The texture analyzer, J. Microsc. 95 (1977) 349–356.
[18] C. Lantuejoul, F. Maisonneuve, Geodesics methods in image analysis, Pattern Recognition 17 (1984) 117–187.
[19] P.F. Leonard, Pipeline architecture for real time machine vision, in: Proceedings of the IEEE Comp. Soc. Workshop on Computer Architecture for Pattern Analysis and Image Database Management, 1985, pp. 502–505.
[20] L.M. Lifshitz, S.M. Pizer, Multiresolution hierarchical approach to image segmentation based on intensity extrema, IEEE Trans. Pattern Anal. Mach. Intell. 12 (6) (June 1990) 529–540.
[21] P. Maragos, Pattern spectrum and multiscale shape representation, IEEE Trans. Pattern Anal. Mach. Intell. PAMI-11 (1989) 701–716.
[22] P. Maragos, R.W. Schafer, Morphological filters — Part II: their relations to median, order-statistics, and stack filters, IEEE Trans. Acoust. Speech and Signal Process. ASSP-35 (8) (August 1987) 1170–1184.
[23] G.M. Matheron, Random Sets and Integral in Geometry, Wiley, New York, 1975.
[24] F. Meyer, Contrast feature extraction, in: J.L. Chermant (Ed.), Quantitative Analysis of Microstructures in Material Sciences, Biology and Medicine, Riederer Verlag, Stuttgart, Germany, 1978.
[25] H. Minkowski, Volume and oberflache, Math. Ann. 57 (1903) 447–495.
[26] S. Mukhopadhyay, B. Chanda, A multiscale morphological approach to local contrast enhancement, Signal Processing 80 (April 2000) 685–696.
[27] P. Perona, J. Malik, Scale-space and edge detection using anisotropic diffusion, IEEE Trans. Pattern Anal. Mach. Intell. 12 (7) (July 1990) 629–639.
[28] C.C. Pu, F.Y. Shih, Threshold decomposition of grey-scale soft morphology into binary soft morphology, CVGIP-Graph. Models Image Process. 57 (6) (1995) 522–526.
[29] A. Rosenfeld, A.C. Kak, Digital Picture Processing, 2nd Edition, Vols. 1 & 2, AP, NY, 1982.
[30] F. Safa, G. Flouziat, Speckle removal on radar imagery based on mathematical morphology, Signal Processing 16 (1989) 319–333.
[31] P. Salembier, Morphological multiscale segmentation for image coding, Signal Processing 38 (1994) 359–386.
[32] P. Salembier, J. Serra, Flat zones filtering, connected operators and filters by reconstruction, IEEE Trans. Image Process. 8 (4) (August 1995) 1153–1160.
[33] D. Schonfeld, J. Goutsias, Optimal morphological pattern restoration from noisy binary images, IEEE Trans. Pattern Anal. Mach. Intell. PAMI-13 (1991) 14–29.
[34] C.A. Segall, S.T. Acton, Morphological anisotropic diffusion, Proceedings of the 1997 IEEE International Conference on Image Processing, Santa Barbara, CA, October 26–29, 1997, pp. III-348–351.
[35] J. Serra, Image Analysis Using Mathematical Morphology, Academic Press, London, 1982.
[36] X. Song, Y. Neuvo, Robust edge detector based on morphological filters, Pattern Recognition Lett. 14 (1993) 889–894.
[37] S.R. Sternberg, Gray scale morphology, Computer Graphics and Image Processing 35 (1986) 335–355.
[38] A. Toet, A hierarchical morphological image decomposition, Pattern Recognition Lett. 11 (4) (April 1990) 267–274.
[39] L. Vincent, Morphological area openings and closings of greyscale images, Workshop on Shape in Picture, NATO, 1992.
[40] L. Vincent, Morphological area openings and closings for gray-scale images, in: NATO (Ed.), Workshop on Shape in Picture, 1992, pp. 197–208.
[41] L. Vincent, Gray-scale area openings and closings, their efficient implementation and applications, in: Jean Serra, Phillipe Salembier (Eds.), Proceedings of the International Workshop on Mathematical Morphology and its Applications to Signal Processing, May 1993, pp. 22–27.
[42] J. Weickert, A review of non-linear diffusion filtering, Scale-space Theory in Computer Vision, Lecture Notes in Computer Science, Vol. 1252, Springer, Berlin, Invited paper, 1997, pp. 3–28.
[43] W. Wu, M.J. Wang, C. Liu, Performance evaluation of some noise reduction methods, Graph. Models Image Process. 54 (2) (March 1992) 134–146.